Extracting Patterns of Lymphocyte Fluorescence from Digital Microscope Images

Tim W. Nattkemper[1]
Helge Ritter[1], Walter Schubert[2,3]

[1]Neuroinformatics Group, University of Bielefeld, Germany, email: tnattkem@techfak.uni-bielefeld.de
[2]Neuroimmunology and Molecular Pattern Recognition Group, University of Magdeburg
[3]MELTEC Ltd., University of Magdeburg, email:schubert@pc.mdlink.de

Abstract

A system for full-automatic extraction of fluorescence information from lymphocytes in digital microscope images is presented. It is applied on samples of lymphocytes invading muscle tissue. From a single sample images are taken using n different fluorochrome antibody markers. In every image a different subset of the lymphocytes appears through fluorescence. The fluorescent cells in every image are detected by an artificial neural network. After detection, corresponding fluorescences of each cell in different images are collected in lists of length n, called marker combination patterns. Each binary element of a pattern represents, if a cell was fluorescent (1), or not (0) in a particular image. The whole algorithm of detection and correspondence analysis is easy to adapt and computes fast. This automation allows us to gain reproducible data and opens the door for a statistical analysis of a large number of fluorescence patterns.

1 Introduction

In our work we focus on extracting multi-dimensional information about the fluorescence behavior of lymphocyte cells from microscope images.
A fluorescence microscope technique [Schubert, 1992] delivers a stack of n images of a single sample by preparing it with n different fluorochrome markers $m_i, i = 1, \ldots, n$. In every image different subsets of the lymphocytes are fluorescent and appear with shining boundaries. Every lymphocyte in the sample has its specific fluorescence behavior in the image stack. It is fluorescent in a subset of images and is invisible in the rest of the stack. We want to collect the different fluorescences for each lymphocyte in n-dimensional binary lists (see fig. 1). The ith element of a lymphocytes list denotes if the cell was fluorescent in the ith image (1) or not (0). The binary list of a cell is called its marker combination pattern

$$\mathbf{p}_j = (f_1^{(i)}, .., f_n^{(i)}), f_i^{(i)} \in \{0, 1\}.$$

To extract the fluorescence patterns from the image stack the fluorescent lymphocytes in the n images have to be detected. The fluorochrome-marked lymphocytes differ in number, location and intensity, therefore, image parameters like contrast and noise change from image to image. Because the lymphocytes are located in tissue their shape and size show considerable variation. Image interpretation by human employees is infeasible, because it takes to much time and the results are

often unreliable, since the visual inspection is tiresome and makes concentration decrease even after a short time.
Previous related work for automatic cell detection has mainly centered around model-based approaches. Those include the idea of fitting a geometrical model to a gradient ensemble ([Mardia et al., 1997], [Dow et al., 1996]), the use of wave propagation [Hanahara and Hiyane, 1990] or a Hough-transform to detect circle-like objects ([Gerig and Klein, 1986],[Ballard, 1981]). These approaches are often sensitive to changes in the shape of the object and can not be adapted easily by a non-expert. Furthermore, the images are noisy because of heterogeneous light conditions and the cells occlude partially which makes a detection by boundary tracing ([Galbraith et al., 1991]) unsuitable.
Our new approach is a model-free algorithm for cell detection based on neural networks. An artificial neural network computes for every point of an image an evidence value, which describes the degree of belief that a fluorescent cell is centered at this point.
After obtaining the positions of the cells, the complete fluorescence patterns are gained by calculating the correspondences of the cells' positions in the n images. This is done by evaluating the evidences of the neural network of all images to get the positions of all lymphocytes that were fluorescent in at least one image. A simple search for corresponding lymphocyte positions in the n images delivers the desired fluorescence patterns.

2 Multiparameter Fluorescence Imaging

We use fluorochrome markers on lymphocytes to identify the presence of proteins in the cells surface. Each marker binds to a subset of the lymphocytes which depends on the existence of the protein in the lymphocytes membrane. Fluorescence excitation makes the binding lymphocytes appear with high intensities and an image is taken by a CCD-camera. After that, the marker is bleached from the

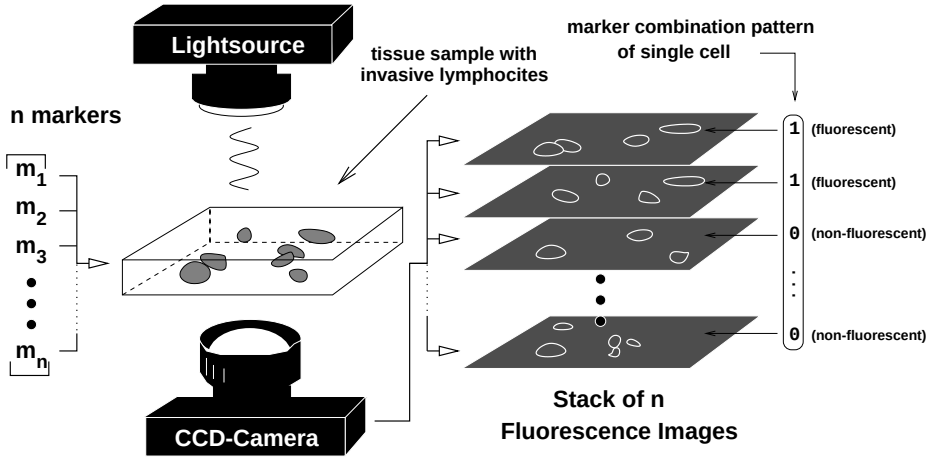

Figure 1: Simplified sketch of the imaging process: The lymphocytes are prepared with n markers in an iterative procedure. At each step, the fluorescence excitation makes those lymphocytes appear in the image that bind to the marker. An intensity image is taken by an integrated CCD-camera. After all n steps are completed a stack of n images with different subsets of lymphocytes can be evaluated.

cells and the process is repeated with another marker. In our system the process of marking, imaging and bleaching can be repeated with up to nine markers (see [Schubert, 1992],[Schubert, 1997] for details). During each repetition the positions of the lymphocytes are not affected, allowing a matching of positions between different images.
In this experimental set-up we analyze T-Lymphocytes invading muscle tissue in case of sarcoid Myopathy. We prepared the lymphocytes with $n = 7$ markers and took seven fluorescence images with different subsets of cells appearing through fluorescence (see fig. 2).

3 Automated Cell Classification

The detection of objects in digital intensity images is a main topic in the field of computer vision and classification. In our work we want to detect cells in noisy grey images in front of dull background. This is interpreted as a classification task. For every point in the image it has to be decided if it is a center of a cell or not. Since the lymphocytes are located in organic fiber during an invasion their shape is not circle- but "potato"-like and is called *mainly convex*. For classification we use a special kind of neural network, called Local Linear Map (LLM) [Ritter, 1991]). The LLM-classificator is trained by a set of image patches containing cells. After training the LLM-classificator computes for every point in the image an evidence value which represents the degree of belief that a fluorescent cell is positioned there. Evaluating the evidences for every marker delivers the desired fluorescence patterns. The whole learning and classification process is described in figure 3 and in the following.

3.1 Training the Classificator

To train the LLM-classificator one image is selected from the image stack. A human expert marks a set of fluorescent cells using a computer mouse. The set of $N \times N$-sized image-patches around these cells builds the set of positive training examples. A second set of patches is selected by random

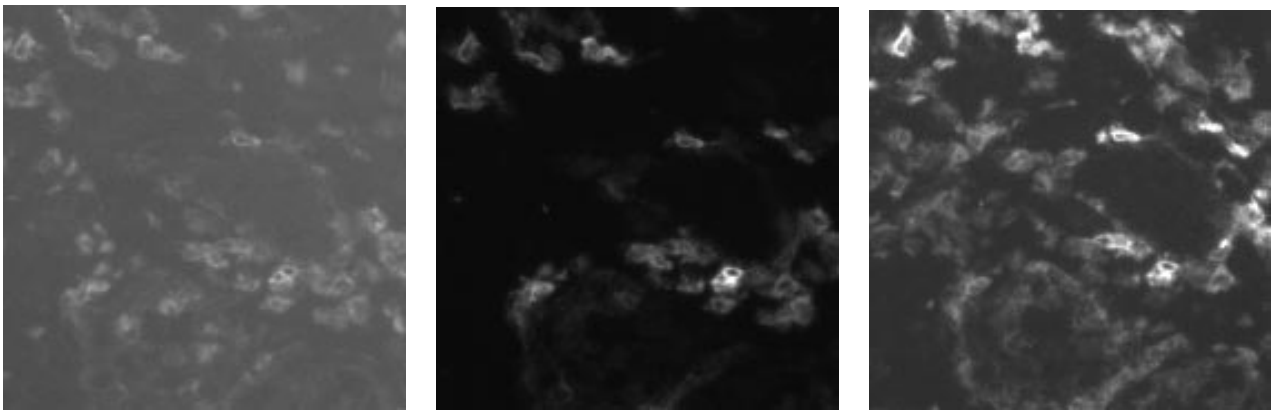

(a) (b) (c)

Figure 2: Clippings from three fluorescence images: The images show identical regions of the sample. One can see, that some fluorescent lymphocytes appear in every image and some only in one or two of them.

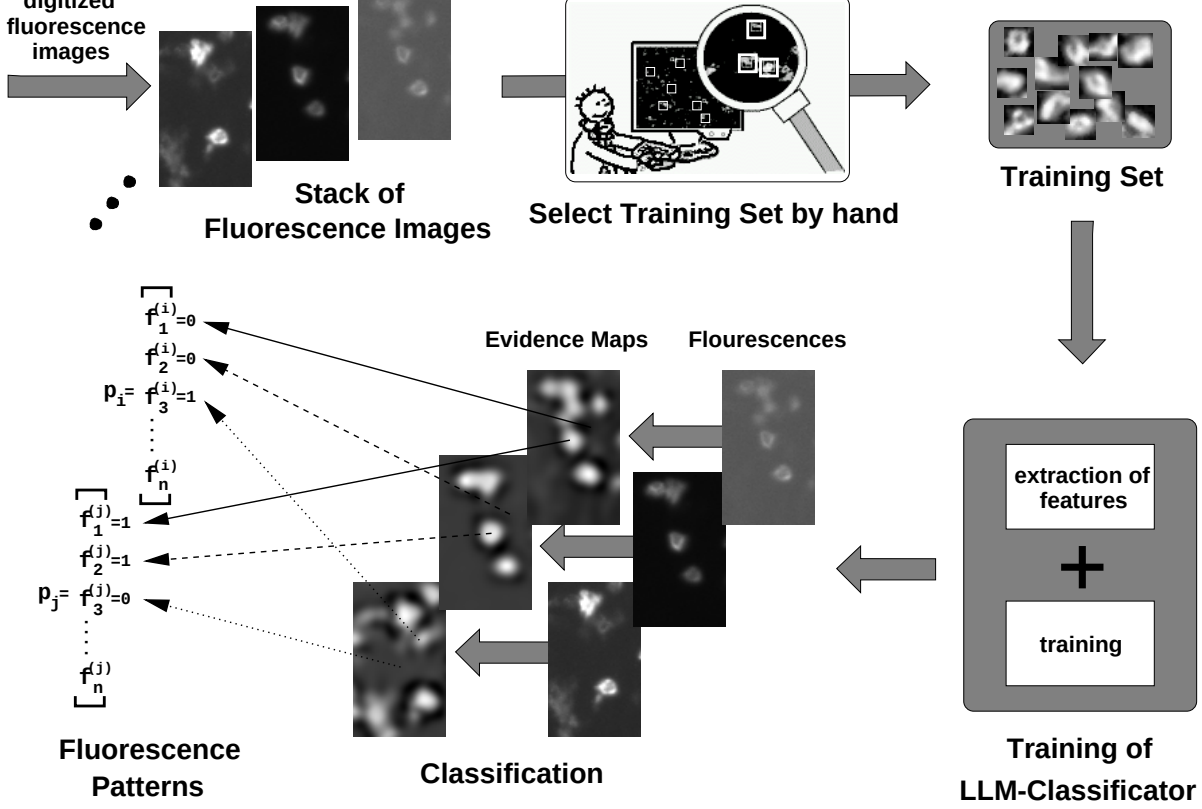

Figure 3: Sketch of the system: Using a mouse an expert selects a set of image points which are centers of cells. These are fed to the LLM-classificator which learns the classification rule. Using the trained classificator the fluorescent cells in every image are detected. After that corresponding fluorescences are collected to the desired binary fluorescence patterns $\mathbf{p}_i$.

full-automatically from the same image with a minimum distance of 5 pixels to the expert-marked regions, which is the set of negative training example patches.
For every training example patch a d_{in}-dimensional feature vector $\mathbf{x}$ is calculated. Therefore, a Principal Component Analysis is carried out on the set of hand-selected cell patches. This is a well-known technique in classification tasks in Computer Vision (see [Turk and Pentland, 1991]for example). The basic idea of PCA is that the high-dimensional image patch is mapped into a much lower dimensional ($d_{in} = 6$) feature space. These features provide the input feature vectors $\mathbf{x}$. Calculating the feature vectors for the positive and the negative input examples delivers the training set of (input, output)-pairs

$$\Gamma = \{(\mathbf{x}_\alpha, \mathbf{y}_\alpha)\}_\alpha.$$

For the positive training set $\mathbf{y}_\alpha$ is set to 1, to 0 for the negative ones.
The LLM is given through

$$\{\mathbf{w}_i^{in} \in \mathbb{R}^{d_{in}}, \mathbf{w}_i^{out} \in \mathbb{R}^{d_{out}}, \mathbf{A}_i \in \mathbb{R}^{d_{in} \times d_{out}}, i = 1..l\}.$$

A triple $\nu_i = (\mathbf{w}_i^{in}, \mathbf{w}_i^{out}, \mathbf{A}_i)$ is called a node. For training the LLM a pair $(\mathbf{x}_\alpha, \mathbf{y}_\alpha)$ is selected from Γ by random and the learning rules

$$\Delta \mathbf{w}_\kappa^{in} = \epsilon^{in}(\mathbf{x}_\alpha - \mathbf{w}_\kappa^{in}) \tag{1}$$

$$\Delta \mathbf{w}_\kappa^{out} = \epsilon^{out}(\mathbf{y}_\alpha - \mathbf{y}(\mathbf{x}_\alpha)) + \mathbf{A}_\kappa \Delta \mathbf{w}_\kappa^{in} \tag{2}$$

$$\Delta \mathbf{A}_\kappa = \epsilon^{A}(\mathbf{y}_\alpha - \mathbf{y}(\mathbf{x}_\alpha)) \frac{(\mathbf{x}_\alpha - \mathbf{w}_\kappa^{in})^T}{\| \mathbf{x}_\alpha - \mathbf{w}_\kappa^{in} \|^2} \tag{3}$$

are carried out. $\epsilon^{in}, \epsilon^{out}, \epsilon^{A} \in]0, 1[$ are decreasing learning step sizes and κ holds $\kappa = \arg\min_k \{\| \mathbf{x} - \mathbf{w}_k^{in} \|\}$. So $\mathbf{w}_\kappa^{in}$ is the next neighbor to input $\mathbf{x}$. This is repeated $l * 10.000$ times.
The trained LLM-classificator performs a mapping of fluorescence image points to evidence values in $[0; 1]$. To calculate the evidence value for a fluorescent cell at one image point the feature vector $\mathbf{x}$ for its surrounding region is calculated and the LLM output for the input $\mathbf{x}$ is computed by

$$\mathbf{y}(\mathbf{x}) = \mathbf{w}_\kappa^{out} + \mathbf{A}_\kappa(\mathbf{x} - \mathbf{w}_\kappa^{in}) \tag{4}$$

$$\text{with } \kappa = \arg\min_k \{\| \mathbf{x} - \mathbf{w}_k^{in} \|\}.$$

In this work the number of nodes is $l = 5$ and the patch size is $N = 15$.

3.2 Detection of fluorescent cells

To detect all fluorescent cells in one image of the stack every image point is mapped to its evidence value by (4). The surrounding image region of the point is given to the classificator which calculates its evidence value. Calculating the evidences for every point of an image gives a so called evidence map of the image (see fig. 4(b)). Regions of large evidences (bright clouds in evidence maps in fig. 4(b)) indicate fluorescent cells in the corresponding fluorescence image. All points with an evidence value larger than 0.5 and no larger evidences in their neighborhood form the set of fluorescent cells' positions in the image (see fig. 4(c)). This is done for all images of the stack.

3.3 Selection of Threshold by ROC

We validate the selection of threshold $t = 0.5$ for the LLM by a Receiver Operator Characteristic (ROC) plot (see [Zweig and Campbell, 1993] for a review). Therefore 20% of the positive examples and 20% of the negative examples were subtracted from the training set Γ. The subtracted examples build the new test set Γ^{test} of (input,output)-pairs. The remaining examples form the new training set Γ^{train}. The LLM is trained as described in section 3.1 with Γ^{train}. After training, for every input $\mathbf{x}$ of Γ^{test} the evidence value $\mathbf{y}(\mathbf{x}) \in [0; 1]$ is calculated by equation (4). If the output holds $\mathbf{y}(\mathbf{x}) > t$ the input vector is classified as a cell (positive), otherwise it is classified as a non-cell (negative). Using the target output values of the inputs the classification rates of true positives (TP) and true negatives (TN) for Γ^{test} were calculated. This was done for 10 different Γ^{test} and the mean values for TP and NP were calculated. The results are shown for $t = 0.0, 0.1, 0.2, \ldots, 1.0$ in figure 4(d). One can see that the LLM performs with similar accuracy on positive and negative examples when t is set to 0.5. Because it is not possible to measure the costs for either false positives or false negatives $t = 0.5$ was selected to ensure homogeneous performance on positive and negative inputs.

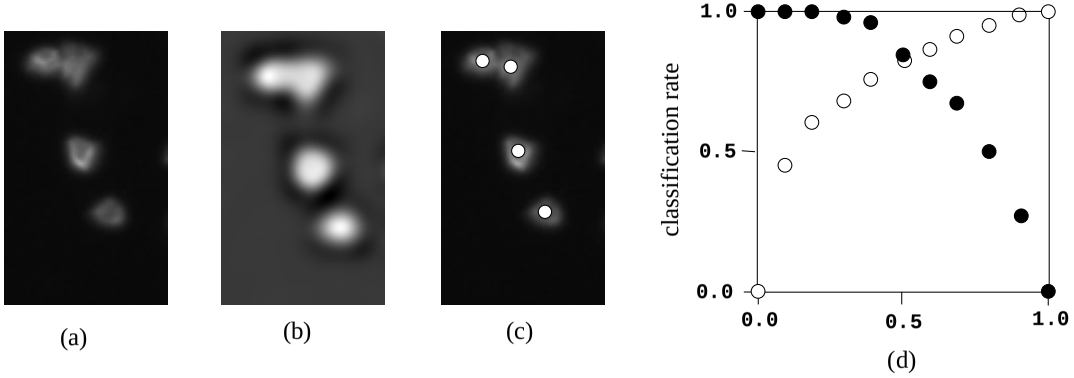

Figure 4: (a)-(c):Detection of fluorescent cells. For every point of an input image (a) the LLM-classificator computes its evidence value. Computation of evidence values for all image points delivers the evidence map (b) (normalised to $[0; 255]$ for better viewing). Thresholding and local maximum search leads to the desired positions (white balls) of fluorescent cells (c). (d): A ROC of the LLM plotted against threshold t. For every t the LLM classification rate on positive and negative training inputs was calculated. For t growing from 0 to 1.0 the rates of true positives (white circles) and true negatives (black circles) are plotted.

3.4 Accuracy of the Detected Cell Positions

To value the accuracy of the cell detection, its rates of false positives and true positives were measured. Therefore, two fluorescence images gained with different markers (`cd3,cd4`) were evaluated by the trained LLM and the detected cell positions were framed by white boxes in the images. This way more than 600 fluorescent lymphocytes were found using the method described in section 3.2 and visualized in both images. The expert with far most experience in evaluating fluorescence images by visual inspection estimated the rate of true positives of the system to be $90 - 95\%$ and the rate of false positives about 5%.

4 Collecting Fluorescence Patterns

After the process of cell detection for all images one has to find locally corresponding fluorescence spots in different images to map fluorescences of the same cell to its marker combination pattern. This correspondence analysis is based only on the cells' positions in the images and is a difficult task because the positions of one cell in different images calculated by the algorithm are not exactly the same. In addition the number of fluorescent cells in the images varies from eight to more than 400. Both makes simple matching based only on the detected cells' positions infeasible. In our algorithm we avoid such problems by evaluating the evidences of all images of the stack.
Calculating the evidences for all n images as described above leads to n evidence values for every point. Now for every point its maximum evidence is selected and is written into a new evidence map at its coordinates. This map is called the *master-evidence map* (see fig. 5) because every lymphocyte which appeared in at least one of the images is represented in this map by a large evidence value. By applying our thresholding procedure, described in sec. 3.2 to the *master-evidence map* we obtain all positions of these lymphocytes. This set of M cell positions $\{(x_i, y_i)\}$ is called the *master set*.
Now for every cell from the *master set* the binary fluorescence values $f_j^{(i)}$ are collected. f_j of

$\mathbf{p}_i = (f_1^{x_i}, .., f_n^{x_i})$ is set to 1 if a cell was detected in the j-th fluorescence image of the stack in a close neighborhood of its coordinates (x_i, y_i). The operation is illustrated in fig. 5.

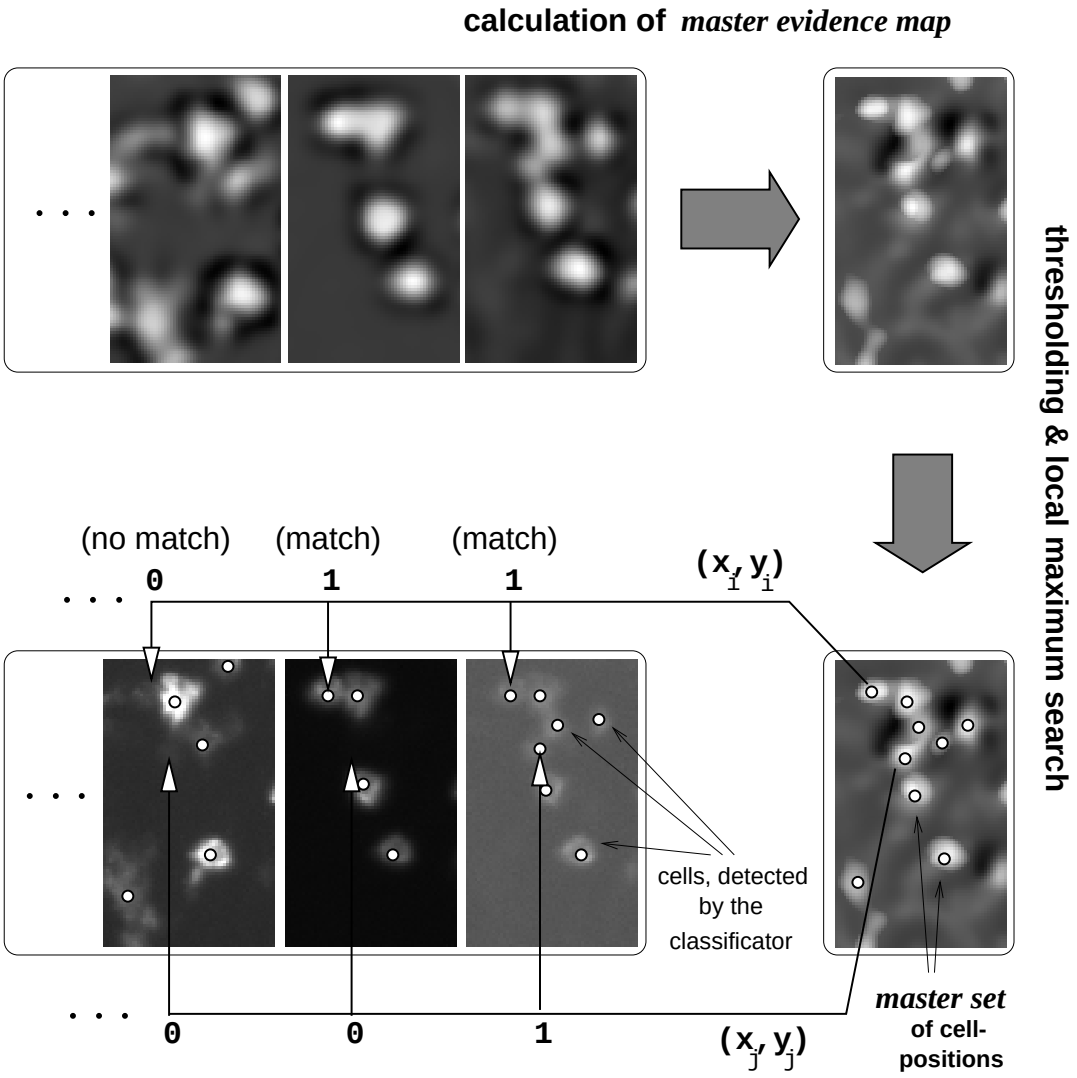

Figure 5: Collecting of marker combination patterns: The maximum evidence values for all points are written to the *master-evidence map*. The positions of all fluorescent cells in all images, the *master set* are extracted from these. A simple local matching procedure between the *master set* and the lists of the cell positions detected for all fluorescence images delivers the binary fluorescence patterns of all detected cells.

5 Results

A stack of seven fluorescence images were taken as described above. The seven different markers are `cd2, cd3, cd4, cd8, cd11b, cd19` and `cd26`, which are common antibody markers in fluorescence microscopy. The training set of cell patches was selected by hand from the `cd4`-image. In every image fluorescent cells were detected by the LLM-classificator. Using the maximum condition on the evidences computed by the LLM the *master evidence map* was assembled. From the *master*

evidence map the positions of $M = 550$ fluorescent cells were extracted. Finally, the local matching step delivered the marker combination patterns $\mathbf{p}_j, j = 1, \ldots, 550$.
To look at the distribution of the marker combination patterns within the set of lymphocytes their binary patterns $(f_1^{(j)}, ..., f_7^{(j)})$ were mapped to a numerical label by simple mapping from the dual system to the decimal system. The frequencies of the patterns were counted and plotted to a histogram of $2^7 = 128$ boxes. The histogram is shown in figure 6. Looking at figure 6 one observes, that only 24 of the 128 possible patterns were found in the whole set of lymphocytes. On first sight three patterns dominate in number, `(1000000)`(=1), `(0010000)`(=8) and `(1010000)`(=9). These are cells which only coupled to the `cd2` or to `cd4` or only to both of them. The rest of the frequencies are less then 30.
To get an impression about the coincidence of a particular marker with remaining ones, for every marker a corresponding histogram was computed (see fig. 7). The black box in the histograms show the absolute number of cells which were fluorescent with this selected marker. The grey boxes show the numbers of cells which were fluorescent with this marker **and** with the (black box-) marker. Looking at the histograms in figure 7 one can see that the absolute numbers of fluorescent cells vary strongly. Most dominant are the markers `cd2` and `cd4`. Lymphocyte fluorescent with marker `cd19` occur seldom and coincide only once with another marker (`cd2`). One can say that this marker is highly selective.
Strong coincidence can e. g. be observed between the pairs `(cd2,cd8)`, `(cd3,cd8)` and `(cd2,cd3)`. A table of all 24 marker combination patterns and their frequencies is given in the appendix.

6 Discussion

In the present example, images recorded from one single visual field was analyzed. Given a large number of several hundred visual fields, it will be possible by our approach to present, within a

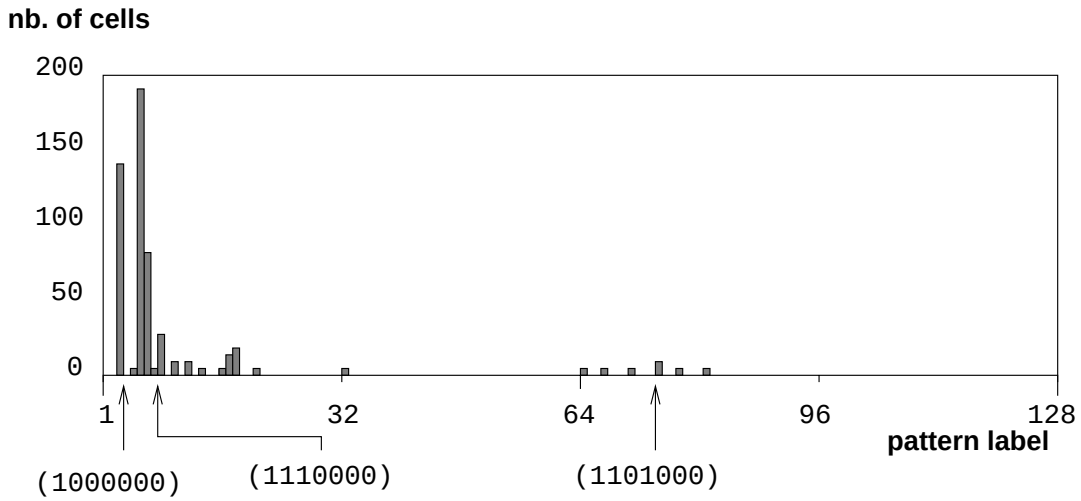

Figure 6: Histogram of the absolute frequencies of the marker combination patterns: The binary patterns were mapped from the dual system to the decimal system to label them. Only a small fraction of 24 possible patterns were found in the whole set of lymphocytes. For illustration, three example patterns are indicated below the label-axis for illustration. Note that 4 of the patterns were only found once so that their frequency is not visualized in this plot.

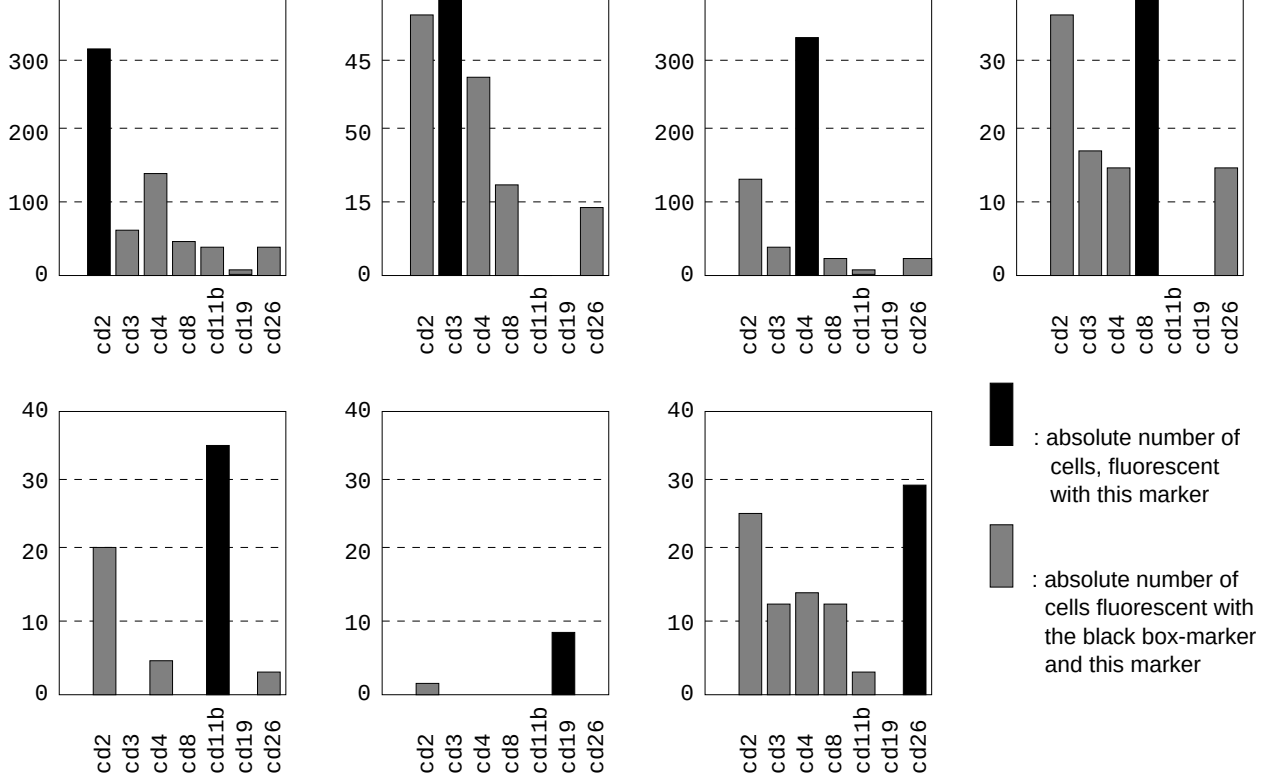

Figure 7: Coincidence histograms for all seven markers: For each marker the absolute number of binding cells is plotted (black boxes). The number of cells with coincident binding with another marker are plotted in the grey boxes. Note the different scaling of the frequency axis for better viewing.

relatively short timescale, a precise statistical analysis of the immune cell subsets that have invaded the sites. The quantitative data show that the most frequent cells are lymphocytes expressing the `cd2` receptor alone or the `cd4` receptor alone, without co-expression of other receptors labeled by our antibody library. This result supports our previous notion, that muscle-invasive lymphocytes express unusual cell surface receptor patterns ([Schubert et al., 1993],[Schubert, 1997]). The present constellation is surprising, because in the periphery, i. e. in blood, cells expressing `cd2`, as a rule co-express `cd3` and co-express either `cd4` or `cd8`. In addition the limited heterogeneity of the immune cells generated by differential combinations of 7 different receptor proteins in the cells (only 24 different subsets) argues for a largely restricted usage of a probably much larger combinatorial program. Hence our multi-parameter approach uncovers hitherto unknown new combinatorial patterns with restricted receptor expressions. It is likely that these patterns are directly linked to the disease specific pathogenetic activity of the cell surfaces of the invasive immune cells interacting with tissue sites.

We present an algorithm that is able to extract quantitative data from stacks of fluorescence images of tissue-invading lymphocytes. The algorithm is easy to adapt to new image stacks because the training of the cell classificator only needs the estimated mean size of the cells and a selected training set. This can easily be done by a non-expert. The computation time for a stack of seven 658×517-images is less then 5 minutes on a standard PC.

We also solve the problem of matching fluorescence of one and the same cell to binary data. This

list in addition to the coordinates of the lymphocyte gives its fluorescence pattern. Full automated collection of the fluorescence patterns of large sets of data opens the door for advanced statistical analysis.

Future work will focus on designing more advanced methods for visualizing the data in connection to the development of data mining tools for this kind of data. In this way we want to get insight into relationships between functionalities of lymphocytes and combinatorics of surface proteins which finally produces insight into the molecular compartmentalization of the lymphocyte system in health and disease at the molecular level of cell surfaces.

7 Acknowledgments

This work was supported by the DFG grants GK-231, SFB-387(TPB1), Schu627/8-2, BMBF-07NBL04(TPB9) and -0311951.

A Table of marker combination patterns

frequency	cd2	cd3	cd4	cd8	cd11b	cd19	cd26
190	0	0	1	0	0	0	0
140	1	0	0	0	0	0	0
82	1	0	1	0	0	0	0
27	1	1	1	0	0	0	0
17	1	0	0	0	1	0	0
11	0	0	0	0	1	0	0
10	1	0	0	1	0	0	0
8	1	1	0	1	0	0	0
7	1	1	0	1	0	0	1
7	1	1	1	0	0	0	1
6	0	0	0	0	0	1	0
5	1	0	1	1	0	0	0
5	1	0	1	1	0	0	1
4	1	1	0	0	0	0	0
4	0	1	1	0	0	0	0
4	0	0	1	0	1	0	0
3	1	0	0	0	0	0	1
2	1	1	1	1	0	0	0
2	0	0	1	0	0	0	1
2	1	0	0	0	1	0	1
1	1	0	1	0	1	0	0
1	1	0	0	0	0	1	0
1	1	0	0	1	0	0	1
1	0	0	1	1	0	0	1

Table of all 24 found marker combination patterns. They are listed in decreasing frequencies computed by our algorithm.

References

[Ballard, 1981] Ballard, D. H. (1981). Generalizing the Hough transform to detect arbitrary shapes. *Pattern Recognition*, 13:111–121.

[Dow et al., 1996] Dow, A., Shafer, S., Kirkwood, J., R.A., M., and Waggoner, A. (1996). Automatic multiparameter fluorescence imaging for determining lymphocyte phenotype and activation status in melanoma tissue sections. *Cytometry*, 25:71–81.

[Galbraith et al., 1991] Galbraith, W., Wagner, M., Chao, J., Abaza, M., Ernst, L., Nederlof, M., Hartsock, R., Taylor, D., and Waggoner, A. (1991). Imaging cytometry by multiparameter fluorescence. *Cytometry*, 12:579–596.

[Gerig and Klein, 1986] Gerig, G. and Klein, F. (1986). Fast contour identification through efficient Hough transform and simplified interpretation strategy. *Proc. Int. Conf. on Pattern Recognition*, 8:498–500.

[Hanahara and Hiyane, 1990] Hanahara, K. and Hiyane, M. (1990). A circle-detection algorithm simulating wave propagation. *Machine Vision and Applications*, 3:97–111.

[Mardia et al., 1997] Mardia, K., Qian, W., Shah, D., and de Souza, K. (1997). An algorithm for dividing clusters fluorescent stained nuclei. *IEEE Transactions on Pattern Analysis and Machine Inteligence*, 19:1035–1042.

[Ritter, 1991] Ritter, H. (1991). Learning with the self-organizing map. In Kohonen, T., editor, *Artificial Neural Networks 1*. Elsevier Science Publishers, B.V.

[Schubert, 1992] Schubert, W. (1992). Antigenic determinants of t-lymphozyte $\alpha\beta$ receptor and other leucocyte surface proteins as differential markers of skeletal muscle regeneration: detection of spatially and timely restricted patterns by MAM microscopy. *Eur. J. Cell Biol.*, 58:395–410.

[Schubert, 1997] Schubert, W. (1997). Molecular semiotic structures in the cellular immune system: key to dynamics and spatial patterning? In J. Parisi, S.C. Mueller, W. Z., editor, *A perspective look at nonlinear media in physics, chemistry and biology, Lecture notes in physics*. Springer, Berlin.

[Schubert et al., 1993] Schubert, W., Masters, C. L., and Bayreuther, K. (1993). App+ t-lymphocytes selectively sorted endomysial tubes in polymyositis displace ncam expressing muscle fibres. *Eur. J. Cell Biol.*, 58:395–410.

[Turk and Pentland, 1991] Turk, M. and Pentland, A. (1991). Eigenfaces for recognition. *Journal of Cognitive Neuroscience*, 3:71–86.

[Zweig and Campbell, 1993] Zweig, H. M. and Campbell, G. (1993). Receiver-operating characteristic (roc) plots: A fundamental evaluation tool in clinical medicine. *Clin. Chem.*, 39(4):561–577.